Joule

CellPress

Article

High-Energy-Density Solid-Electrolyte-Based Liquid Li-S and Li-Se Batteries

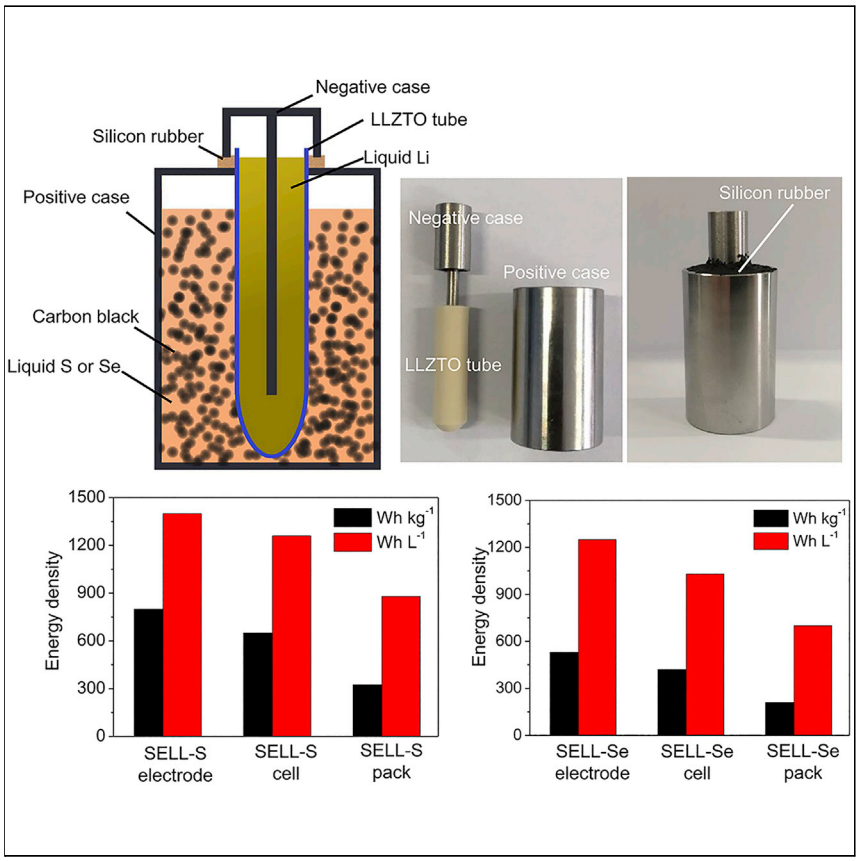

High-energy-density battery systems have been critical to applications in consumer electronics, aviation, electric vehicles, and emerging large-scale stationary storage. Here, we report a solid-electrolyte-based liquid Li-S and Li-Se (SELL-S and SELL-Se in short) battery system with the potential to deliver energy density exceeding 500 Wh kg^{-1} and 1,000 Wh L^{-1}, together with the ability of low cost and stable electrochemical performance for future concentrated and large-scale storage applications.

Yang Jin, Kai Liu, Jialiang Lang, ..., Chang-an Wang, Hui Wu, Yi Cui

huiwu@tsinghua.edu.cn (H.W.)
yicui@stanford.edu (Y.C.)

HIGHLIGHTS

SELL-S and SELL-Se batteries can potentially deliver high energy density of 500 Wh kg^{-1}

Liquid-solid interfaces facilitate rapid ion transport and low interfacial impedance

Polysulfide or polyselenide shuttle effects prevented by the compact ceramic LLZTO tube

Jin et al., Joule 4, 262–274
January 15, 2020
https://doi.org/10.1016/j.joule.2019.09.003

Joule

CellPress

Article

High-Energy-Density Solid-Electrolyte-Based Liquid Li-S and Li-Se Batteries

Yang Jin,[1,2,3,6] Kai Liu,[2,6] Jialiang Lang,[2,6] Xin Jiang,[1,3] Zhikun Zheng,[1,3] Qinghe Su,[1,3] Zeya Huang,[2] Yuanzheng Long,[2] Chang-an Wang,[2] Hui Wu,[2,3,*] and Yi Cui[4,5,7,*]

SUMMARY

Lithium-sulfur (Li-S) and Lithium-selenium (Li-Se) batteries are considered as promising candidates for next-generation battery technologies, as they have high energy density and low cost. However, due to the use of a solid Li-metal anode and a liquid organic electrolyte, the current Li-S and Li-Se batteries face several issues in terms of Coulombic efficiency and cycling stability, which seriously impeded their development. Here, we report solid-electrolyte-based liquid Li-S and Li-Se (SELL-S and SELL-Se in short) batteries. The batteries use a $Li_{6.4}La_3Zr_{1.4}Ta_{0.6}O_{12}$ (LLZTO) ceramic tube as electrolyte and work at temperatures higher than the melting point of Li; thus, polysulfide or polyselenide shuttle effects and Li dendrite growth are effectively prevented, and high energy density, together with high stability, fast charge/discharge capability, high Coulombic efficiency, and high energy efficiency, can be achieved. The SELL-S and SELL-Se batteries provide broader platforms for constructing high-energy, high-power, long-lifetime, and low-cost energy storage.

INTRODUCTION

The current state-of-the-art Li-ion batteries (LIBs) have an energy density of less than 300 Wh kg^{-1} and 750 Wh L^{-1}.[1–3] Sulfur (S) and selenium (Se), which are in the same main group (group VIA) of the periodic table, are promising candidates to replace commercial metallic oxide cathodes for LIBs because of their high capacity (1,670 mAh g^{-1} when lithiated to Li_2S and 675 mAh g^{-1} when lithiated to Li_2Se), high theoretical energy density (~2,600 Wh kg^{-1} and 2,800 Wh L^{-1} for Li-S battery; ~1,160 Wh kg^{-1} and 2,530 Wh L^{-1} for Li-Se battery),[4,5] and correspondingly low cost ($41 kWh^{-1} for Li-Se and $15 kWh^{-1} for Li-S based on electrode materials; Table S1). Since the initial use of S and Se as electrodes in batteries, investigations of Li-S and Li-Se batteries have attracted substantial attention. Previous research has mostly focused on batteries with a solid-state Li-metal anode, a solid-state S or Se cathode (powder or different S/C or Se/C composites), and a liquid organic electrolyte.[6–9] However, due to the use of solid Li metal and a liquid organic electrolyte, the above battery structure has certain intrinsic issues: (1) poor cycling stability and low Coulombic efficiency because of the shuttling effect caused by dissolution of short-chain Li_2S_x or Li_2Se_x in the liquid organic electrolyte, (2) safety issues associated with the high flammability of the liquid organic electrolyte, and (3) dendritic growth of the Li anode and its side reactions in the electrolyte.[10–13] Additionally, a large volume change of solid S and Se during charge and discharge causes the abscission of active S or Se from the current collector, causing cycling instability and decreasing the usage of Se and S.[14–18] These issues have seriously impeded the development of Li-S and Li-Se batteries.

Context & Scale

The current state-of-the-art Li-ion batteries (LIBs) have an energy density of less than 300 Wh kg^{-1} and 750 Wh L^{-1}. A reliable battery system with an energy density higher than 500 Wh kg^{-1} and 1,000 Wh L^{-1} has yet to be developed to meet with the long-term demands. Here, we report solid-electrolyte-based liquid Li-S and Li-Se (SELL-S and SELL-Se in short) battery systems, which have the potential to deliver energy density exceeding the above needs. Additionally, as the batteries have no polysulfide or polyselenide shuttle effects and no Li dendrite growth, the devices present high Coulombic efficiency and energy efficiency of ~99.99% and ~85%, respectively. The SELL-S and SELL-Se battery system here provide broader platforms for constructing high-energy, high-power, long-lifetime, and low-cost energy storage.

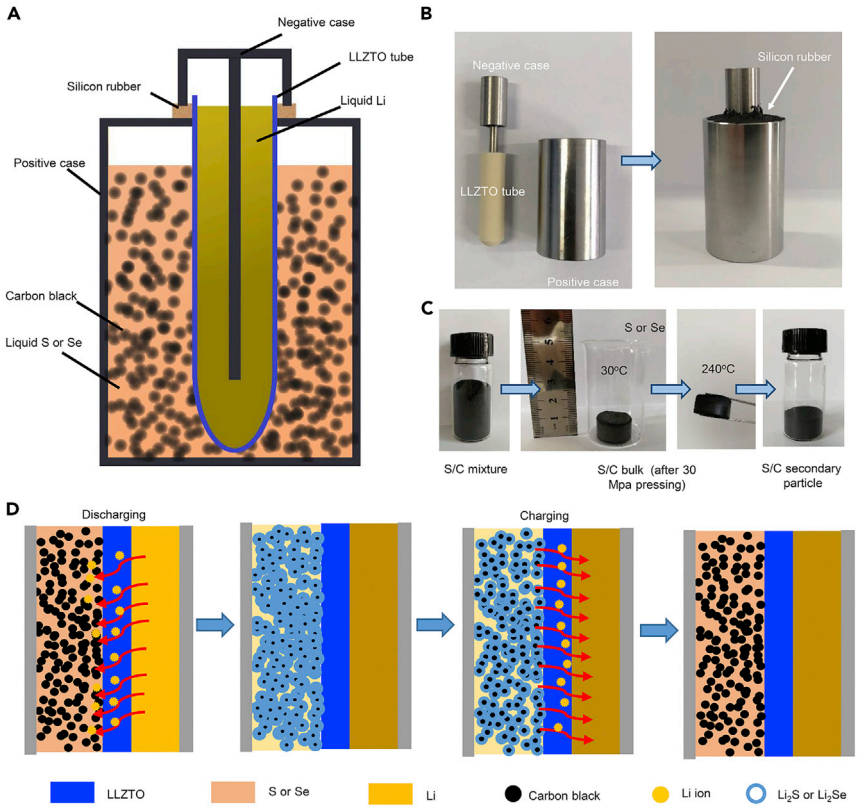

Figure 1. Structure and Schematic Diagram of SELL-S and SELL-Se Battery System

(A) Structure of the SELL-S and SELL-Se batteries. Cross section of the battery.

(B) Optical image of a SELL-S and SELL-Se cell case.

(C) Process of S/C secondary particle preparation using isotactic cool pressing.

(D) Charge and discharge schematic of SELL-S and SELL-Se batteries.

To address the above issues related to the liquid organic electrolyte, here we proposed and designed SELL-S and SELL-Se battery system with ceramic solid electrolyte tubes. Recently, we demonstrated a liquid battery consisting of a garnet-type $Li_{6.4}La_3Zr_{1.4}Ta_{0.6}O_{12}$ (abbreviated as LLZTO) solid electrolyte, a liquid Li-metal anode, and liquid Sn-Pb or Bi-Pb cathodes for grid-scale storage, although their energy density is limited.[19] Here, we expand this architecture to high-capacity Li-S and Li-Se battery chemistries for achieving high energy density.

RESULTS

Schematic and Design of SELL-S and SELL-Se Batteries

The schematic of the battery configuration is shown in Figure 1A. It consists of a liquid Li-metal anode, a molten S (Se) cathode with carbon black, and an LLZTO ceramic tube electrolyte. Li-metal anode is inside the LLZTO tube, and a stainless steel rod is inserted, serving as the current collector for the anode (Figure 1B). A S(Se) cathode with a carbon black conductive additive (with a mass ratio of m(S or Se):m(C) = 9:1) is inserted into the stainless steel cylindrical container outside the LLZTO tube, being physically and electronically separated from the Li anode by the LLZTO tube. The stainless steel cylinder works as current collector for the cathode at the same time. It is noted that the conductive carbon needed for molten S and Se only occupies 10% of the total electrode weight, so the dead weight is minimized. In our experiment, secondary S/C or Se/C particles were prepared to improve the

[1]School of Electrical Engineering, Zhengzhou University, Zhengzhou 450001, P.R. China

[2]State Key Lab of New Ceramics and Fine Processing, School of Materials Science and Engineering, Tsinghua University, Beijing 100084, P.R. China

[3]Research Center of Grid Energy Storage and Battery Application, Zhengzhou University, Zhengzhou 450001, P.R. China

[4]Department of Materials Science and Engineering, Stanford University, Stanford, CA 94305, USA

[5]Stanford Institute for Materials and Energy Sciences, SLAC National Accelerator Laboratory, 2575 Sand Hill Road, Menlo Park, CA 94025, USA

[6]These authors contributed equally

[7]Lead Contact

*Correspondence: huiwu@tsinghua.edu.cn (H.W.), yicui@stanford.edu (Y.C.)

https://doi.org/10.1016/j.joule.2019.09.003

contact between active materials and LLZTO tube. As shown in Figure 1C, high-pressure isotactic cool-pressing method was used to prepare the S/C or Se/C electrode. After pressing and crush, the density of the secondary electrode is highly improved. The S powder contacts well with the carbon black framework. Even at 240°C, where S is in a molten state, the framework structure is maintained.

The assembled Li||LLZTO||S and Li||LLZTO||Se cells were tested at temperatures of 240°C and 300°C, which are above the melting points of both electrode materials (Figure S1). Li_2S or Li_2Se particles formed on the surface of carbon black framework during the discharging process and turn to liquid S or Se during the charging process (Figure 1D). The intact secondary electrode guarantees the ionic and electronic conductivity.

As the operation temperature was above the melting points of Li, S, and Se, both the anode and cathode materials were liquid, facilitating rapid ion transport and low electrode-electrolyte interfacial impedance, as liquid-solid interfaces were formed rather than solid-solid interfaces. A garnet-type ceramic electrolyte was chosen for its stability against molten Li, which was verified from the X-ray diffraction (XRD) result (Figure S2) of aging experiments and scanning electron microscopy (SEM) measurement of LLZTO tube surface and cross section before and after cycling (Figures S3 and S4).[20–25] In addition, with an elevated operation temperature, the ionic conductivity of garnet-type solid electrolytes increases to a competitive level for fast ion transfer. At 240°C, the ionic conductivity of the LLZTO electrolyte was 135 mS cm^{-1} (Figures S5 and S6) by electrochemical impedance spectroscopy (EIS) analysis (Figures S7–S10), which is much higher than that at room temperature (0.7 mS cm^{-1}). At 300°C, the ionic conductivity increased to 190 mS cm^{-1}. Notably, the ionic conductivities of common organic liquid electrolytes at room temperature are approximately 10 mS cm^{-1}, taking 1 mol $LiPF_6$ salt in a 1:1 ethylene carbonate-ethyl methyl carbonate electrolyte at 30°C as an example.[26] The high ion conductivity of the LLZTO tube at the elevated temperature provides a solid foundation for the high power capability of the cells.

Additionally, the garnet-type electrolyte tube also serves as an insulation layer between the liquid Li and liquid S or Se, which means that penetration and leakage should be completely prevented. Based on our measurements (Archimedes method with ethanol), the relative density of the LLZTO tube is as high as 99%, indicating that the garnet-type solid electrolyte is highly dense. The morphology of the surface and cross section as measured by SEM of the tube confirmed the density of the structure (Figure S11). A nitrogen impermeability test was also conducted by using LLZTO tube (Figure S12), and it verified the impermeability of the tube. Such a high relative density and good impermeability allow the LLZTO tube to prevent any leakage or crossover between the liquid electrodes (no shuttle effect and no Li dendrite formation), ensuring the safety and reliability of the battery and a negligible self-discharge rate.

Characterization of SELL-S and SELL-Se Batteries

Here, the cyclic voltammetry (CV) measurement was also conducted to demonstrate the electrochemical reaction of the S and Se-based cathodes during cycling. For SELL-S battery, it can be seen from Figure 2A that the reduction process occurs at about 2.0 V, which indicates the formation of Li_2S, and the corresponding oxidation process occurs at about 2.4 V (Li_2S turn into S). For SELL-Se battery, it can be seen from Figure 2B that the reduction process occurs at about 1.9 V, and the corresponding oxidation process occurs at about 2.2 V. Another small redox peak exists at about 1.6 V, which may be related to some intermediate Li-Se alloy. This redox peak can

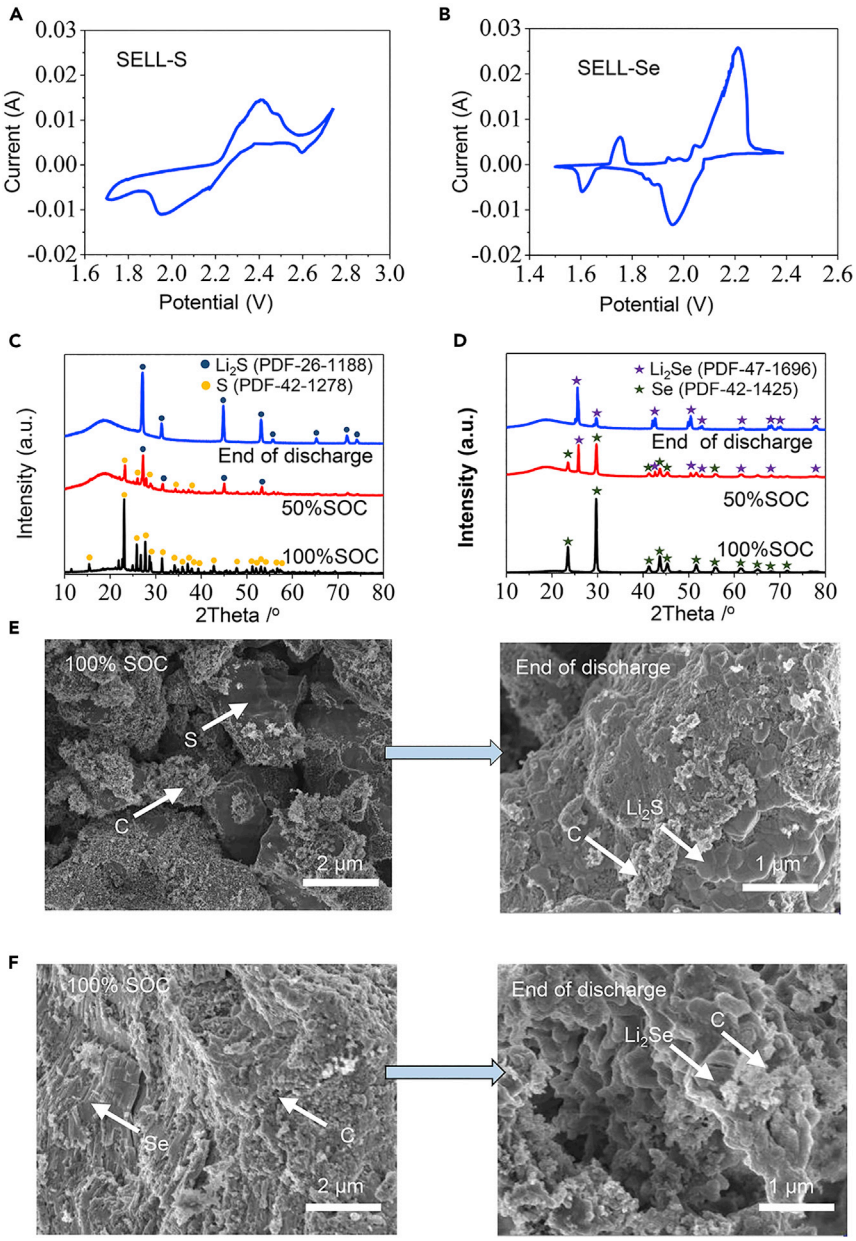

Figure 2. Characterization of SELL-S and SELL-Se Battery System

(A) Cyclic voltammetry (CV) measurement of the SELL-S batteries. (B) Cyclic voltammetry (CV) measurement of the SELL-Se batteries.

(C) X-ray diffraction (XRD) measurement of SELL-S battery at different state of charge (100% SOC and 50% SOC and end of discharge). (D) X-ray diffraction (XRD) measurement of SELL-Se battery at different state of charge (100% SOC and 50% SOC and end of discharge).

(E) SEM image of S/C electrode at 100% SOC and end of discharge.

(F) SEM image of Se/C electrode at 100% SOC and end of discharge.

also be verified in the voltage profile of Li-Se battery, and a small plateau can be observed at about 1.6 V. It is noted that this redox reaction is reversible.

XRD measurement was conducted to demonstrate the intermedia products of the S and Se-based cathodes during charging and discharging. It can be seen from

Figure 2C that with discharging, S was lithiated to Li_2S, with no polysulfide intermediate. At 50% SOC (state of charge), XRD result shows S and Li_2S exist together, and at 100% SOC, mainly Li_2S exists. It can be seen from Figure 2D that with discharging, Se was lithiated to Li_2Se. At 50% SOC, XRD result shows Se and Li_2Se exist together, and at 100% SOC, mainly Li_2Se exists. SEM measurement was conducted to demonstrate the morphology of active materials during charge/discharge. It can be seen from Figures 2E and 2F that at the end of the discharge process, the formed Li_2S adheres strongly with the carbon framework, which can be verified from the following SEM image. This means that Li_2S and Li_2Se particles are formed *in situ* in the framework of S/C and Se/C electrode, which improves the electronic and ionic conductivity of Li_2S and Li_2Se particles to guarantee the reversibility of the reactions. The formed Li_2S/C and Li_2Se/C electrode layers contact tightly with the LLZTO electrolyte with no obvious gap (Figures S13 and S14), which improve the Li-ion transfer at the electrode/electrolyte interface during the charge process.

It is known that the S cathode has a higher Li storage capacity and delivers more energy density than can be achieved with the Se cathode. However, the Se cathode has several advantages over the S cathode, such as a much higher electronic conductivity and lower vapor pressure at elevated temperatures. Compared with S, Se has a much lower vapor pressure (Figure S15), which means that the risk of major leakage is significantly decreased, and accordingly, the sealing requirements and cost will be substantially reduced. To make a clear comparison, a volatilization experiment was conducted. Identical amounts (1 g) of Se and S in open glass containers were transferred to an oven under an argon atmosphere at 300°C, and then the mass variations were measured. These results (Figure S16) show that almost no mass variation occurred for Se, but for S, the mass decreased drastically to almost zero in 6 days. The low vapor pressure of Se results in substantially lower sealing requirements for the SELL-Se battery.

Electrochemical Performance of SELL-S Battery at 240°C

To verify the electrochemical properties, SELL-S cells were assembled and tested at 240°C. The voltage profiles (Figures 3A and 3C) show that the discharge and charge plateaus are ~2.00 V and ~2.10 V, respectively. Figure 3B shows the long cycling performance. During the 50 cycles at a rate of 0.5 C, the performance of the Li|| LLZTO||S cell is stable and shows a gravimetric capacity of approximately 1,450 mAh g^{-1} (91% usage ratio of S). The stable Coulombic efficiency can reach 99.99%, which indicates that the side reactions of the electrode with the LLZTO tube or crossover through the LLZTO tube is negligible. The energy efficiency is approximately 89%. The discharge capacity of SELL-S battery increases in the first 25 cycles. This phenomenon could be due to the activation of S/C electrode at the working temperature of 240°C. Limited by the ionic conductivity of S and the framework of carbon black, the S/C electrode need some cycles to fully contribute to the cell capacity. Figure 3D shows the C-rate cycling performance from 0.5 to 3 C at 240°C. At 3 C, the gravimetric capacity can reach approximately 750 mAh g^{-1} (47% usage ratio of S). In our experiment, the high capacity can be maintained over 50 cycles in SELL-S cells. Further improvement can be realized by better sealing of the S vapor in the future. EIS measurement was also conducted during the discharge and charge process of SELL-S battery. It can be seen from Figures 3E and 3F that during discharge process, with the formation of Li_2S, the resistance of the cell is getting smaller, which could attribute to the higher ionic conductivity of Li_2S than S. At the end of discharge state, the cell resistance is still very small. During charge process, with the Li_2S turn into S, the resistance of the cell is getting bigger. At the end of the charging state (100% SOC), the cell resistance is almost the same as

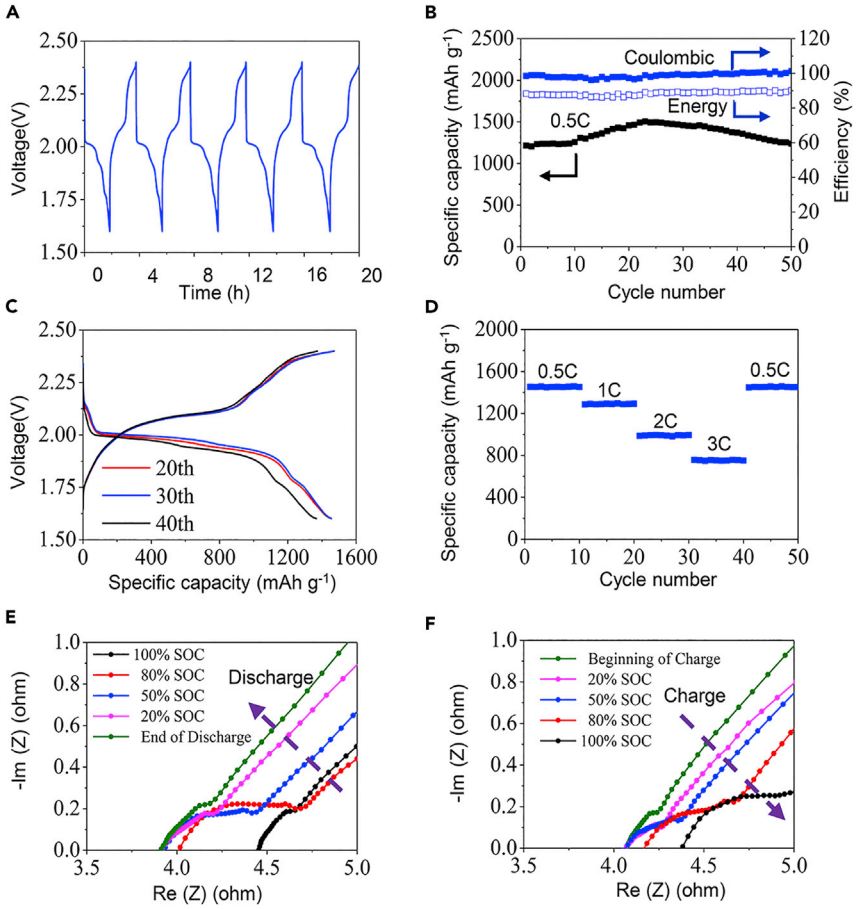

Figure 3. Electrochemical Performance of a SELL-S Cell Operating at 240°C

The mass of active S in each cell is 10 mg, and the inner diameter of the LLZTO tube is 5 mm.

(A) Voltage profiles during charge-discharge cycling from the 1st to 5th cycle at a current density of 8 mA cm^{-2}.

(B) Coulombic efficiency, energy efficiency, and specific capacity as a function of cycle number at a current density of 8 mA cm^{-2}.

(C) Representative voltage profiles during the 20th, 30th, and 40th charge-discharge cycles.

(D) C-rate performance of a SELL-S cell.

(E and F) Electrochemical impedance spectroscopy (EIS) measurement (0.1 Hz–1 MHz) of a SELL-S cell at different state of charge during the discharging process (E) and charging process (F).

the previous 100% SOC. It means that the cell resistance variation is reversible. At the end of discharge state, there is still some molten S or Se existing on the interface as the practical capacity is still smaller than the theoretical capacity, which can help improve the interfacial contact between Li_2S/Li_2Se and LLZTO.

Electrochemical Performance of SELL-Se Battery at 240°C and 300°C

The electrochemical results also verified the excellent electrochemical performance of the SELL-Se cell at 240°C. The voltage profiles in Figures 4A and 4B show that the discharge and charge plateaus are ~2.04 V and ~2.12 V, respectively, which means that the overpotential is just 8 mV at a rate of 1 C (equal to 30 mA cm^{-2}). Figure 4C shows the voltage profiles at different rates. Even at 3 C, the gravimetric capacity can reach as high as 560 mAh g^{-1} (83% usage ratio of Se). Figure 4D shows the long cycling performance. During the 300 cycles at a rate of 1 C, the performance of the SELL-Se cell is very stable, and it shows a gravimetric capacity of approximately 650 mAh g^{-1} (96% of

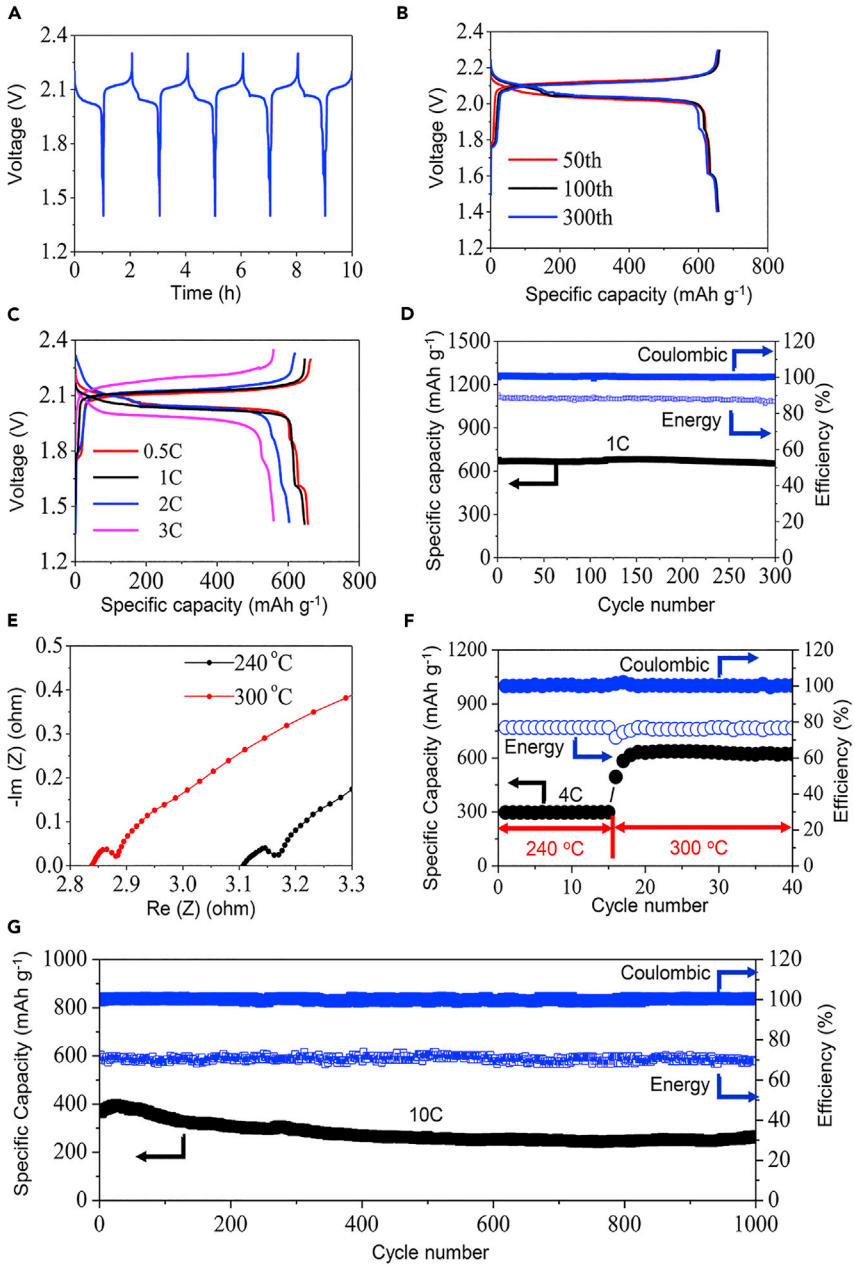

Figure 4. Electrochemical Performance of a SELL-Se Cell Operating

The mass of active Se in each cell is 15 mg, and the inner diameter of the LLZTO tube is 5 mm.

(A) Voltage profiles during charge-discharge cycling from the 1st to 5th cycle at a current density of 10 mA cm^{-2} at 240°C.

(B) Representative voltage profiles during the 50th, 100th, and 300th charge-discharge cycles at 240°C.

(C) C-rate performance of a SELL-Se cell at 240°C.

(D) Coulombic efficiency, energy efficiency, and specific capacity as a function of cycle number at 240°C (1C, current density of 10 mA cm^{-2}).

(E) Electrochemical impedance spectroscopy (EIS) measurement of a SELL-Se cell from 240°C to 300°C (0.1 Hz–1 MHz).

(F) Coulombic efficiency, energy efficiency, and specific capacity variation when the operation temperature is increased from 240°C to 300°C at 4 C and at current density of 40 mA cm^{-2}.

(G) Coulombic efficiency, energy efficiency, and specific capacity as a function of cycle number at 300°C (10 C, current density of 100 mA cm^{-2}).

the theoretical capacity of Se). The capacity decay was very small (~0.004% per cycle) throughout the test. The average Coulombic efficiency was as high as 99.99% (much higher than that of cells using an organic electrolyte, which is approximately 98%), which indicates that the side reaction of the electrode with the LLZTO tube and crossover through the LLZTO tube are negligible. The energy efficiency is stable at 87%. These results confirm the feasibility and reliability of this battery design and further prove the stability of the LLZTO tube. The main discharge plateaus decline slightly from 0.5 to 2 C and down to 2.00 V when the rate increased to 3 C. The cell was cycled 500 times at a rate of 3 C, as shown in Figure S17. The performance of the cell was very stable and showed an average gravimetric capacity of approximately 500 mAh g^{-1} (74% usage ratio of Se). The average Coulombic efficiency was 99.99%, and the energy efficiency was 80%. The cell had a high power capability at 240°C, which can be attributed to the fast Li-ion diffusion in the electrolyte, electrodes, and their interfaces. The fast Li-ion diffusion in the molten Se cathode can be explained based on the Li-Se phase diagram (Figure S1). As seen in the diagram, molten Li has a small but non-negligible solubility in molten Se above 221°C, which means that Li-saturated molten Se (with a Li concentration of ~0.3 mol L^{-1}) will exist in the cathode when the cathode Li:Se mole ratio is <2. If a sufficient concentration of Li atoms is present in the molten Se, they could act as carriers and improve the diffusion of Li ions in the cathode during cycling.

In some specific applications, discharge or charge processes need to be completed in a very short time, such as the fast charge mode of electric vehicles, which is difficult for organic-electrolyte-based batteries because thermal dissipation becomes an issue. In our current battery design, stable cycling at an even higher rate can be easily realized through regulation of the operation temperature. When the operation temperature was increased to 300°C, the Li-ion conductivity and charge transfer kinetics of the LLZTO tube could be significantly increased compared with those at 240°C. Figure 4E shows the EIS measurement result of a SELL-Se cell from 240°C to 300°C. It can be seen that with the working temperature increasing from 240°C to 300°C, the cell resistance was largely reduced, which improves the reaction activity and accelerates the Li-ion transfer speed across the electrode and LLZTO electrolyte.

The electrochemical performance of SELL-Se at 300°C was investigated. As shown in Figure 4F, when the operation temperature was increased from 240°C to 300°C, the gravimetric capacity noticeably increased from 300 mAh g^{-1} to 640 mAh g^{-1} at 4 C, indicating a much better rate performance. Figure S18 demonstrates that at a high rate (4 C), the cell remains stable in a cycling test involving 400 cycles. The average gravimetric capacity is approximately 640 mAh g^{-1} (95% usage ratio of Se). The average Coulombic efficiency remains as high as 99.99%, and the energy efficiency is approximately 80%. Figure S19 shows the C-rate cycling performance from 0.5 to 10 C at 300°C. Even at a high rate of 10 C (100 mA cm^{-2}), which is equal to 180 mW cm^{-2}, a gravimetric capacity as high as 400 mAh g^{-1} (60% usage ratio of Se) is obtained. Figure 4F shows the cycling stability at 10 C. Even after 1,000 cycles, the gravimetric capacity is still approximately 300 mAh g^{-1} (44% usage ratio of Se). The rate and long cycling performance confirm the high power capability and stability of the battery system.

Freeze and Thaw Test

A freeze/thaw test was conducted from 240°C to 20°C during discharge/charge. The result can be seen in Figure S20. After freezing and thawing, regardless of the charging or discharging process, the cell worked normally with no open or short circuit, and no fluctuation in the cycle curves was observed, which means that no mechanical or electrochemical failure of the LLZTO tube occurred. The cell is tolerant of freeze/thaw cycles. The ability of the cell to recover after freezing is of great importance for practical

applications. A self-discharge test was also conducted. With a standing at a working temperature of 300°C for 10 days between full charge and full discharge, the SELL-Se cell still showed a high Coulombic efficiency and energy efficiency of 99.9% and 88%, respectively (Figure S21). The result confirmed no self-discharge happened, indicating that the LLZTO solid electrolyte tube can well separate the anode from the cathode, and there is no leakage or shuttle effects.

Conclusions

Energy Density Calculation

The battery design is feasible for achieving the high energy densities typical of Li-S (Se) batteries due to its architectural simplicity, a significant reduction in the weight of the inactive components, and elimination of the problems associated with traditional liquid electrolyte cells. We also emphasize that the heating and insulation will not obviously affect the volumetric and gravimetric energy densities. Taking the ZEBRA battery as an example, which works at temperatures of 270°C–350°C, the energy density of ZEBRA cell (excluding heating part) is about 120 Wh kg^{-1}, while the ZEBRA pack-level (including heating part) energy density is about 90 Wh kg^{-1} (~25% loss). While a ZEBRA electric vehicle is not in use, the thermal energy loss is just about 90 W or 2.16 kWh per day, which will be even less while in use as the internal resistance of the battery coverts resistive losses to heat with 100% efficiency.[27–29] The existing thermal insulation technology lays a good foundation for the pack system integration of the SELL-S and SELL-Se batteries.

Based on the high capacity of both the cathode and anode materials, and taking advantage of the tightly packed battery configuration,[30–32] our solid electrolyte cells can provide a much higher energy density than can be achieved with traditional LIBs, whose energy density have been limited by the Li storage capacity of their oxide cathodes and graphite carbon anodes as well as the existing "sandwich" battery architecture, in which multiple layers of current collector-cathode-separator-anode-current collector are stacked or rolled together, resulting in a large fraction of deadweight (~50%). We calculated the theoretical volumetric and mass energy densities of the SELL-S and SELL-Se cells based on the cell materials including anode, cathode, solid electrolyte and conductive additive (see detailed calculation information in Figures S22 and S23), and the results are plotted in Figure S23. As the results show, with the diameter of the LLZTO tube increasing, the theoretical energy densities of both the batteries increase, and in general, level off at ~1,850 Wh kg^{-1} and 1,780 Wh L^{-1} for the SELL-S cell, and 920 Wh kg^{-1} and 1,570 Wh L^{-1} for the SELL-Se cell, when the diameter is larger than 6 cm (Figure S23). The energy calculation is based on the active volume and mass of the Li anode, S or Se cathode, conductive additive, and LLZTO tube, not including the stainless steel battery case or the heating and thermal insulation equipment. The wall thickness of the LLZTO tube was 1.5 mm, and the densities of the LLZTO tube were set as 5 g cm^{-3}. The weight and volume stainless steel battery case and the heater will reduce the energy density. Here, we make an estimation about the energy density at the cell level (including stainless steel battery case) and pack level (including stainless steel battery case and heater), which can be seen in Figure 5. This value is based on the practical parameter of Na-S and ZEBRA battery. For SELL-S or SELL-Se battery system, even with a 50% energy density loss from cell level to pack level, they still have competitive energy densities.

To further verify the scale-up property, here we fabricate a SELL-Se cell with 400 mg active material (Se), and the cell capacity can get more than 250 mAh. The result can be seen in Figure S24. The voltage profile is almost the same as the previous 15 mg

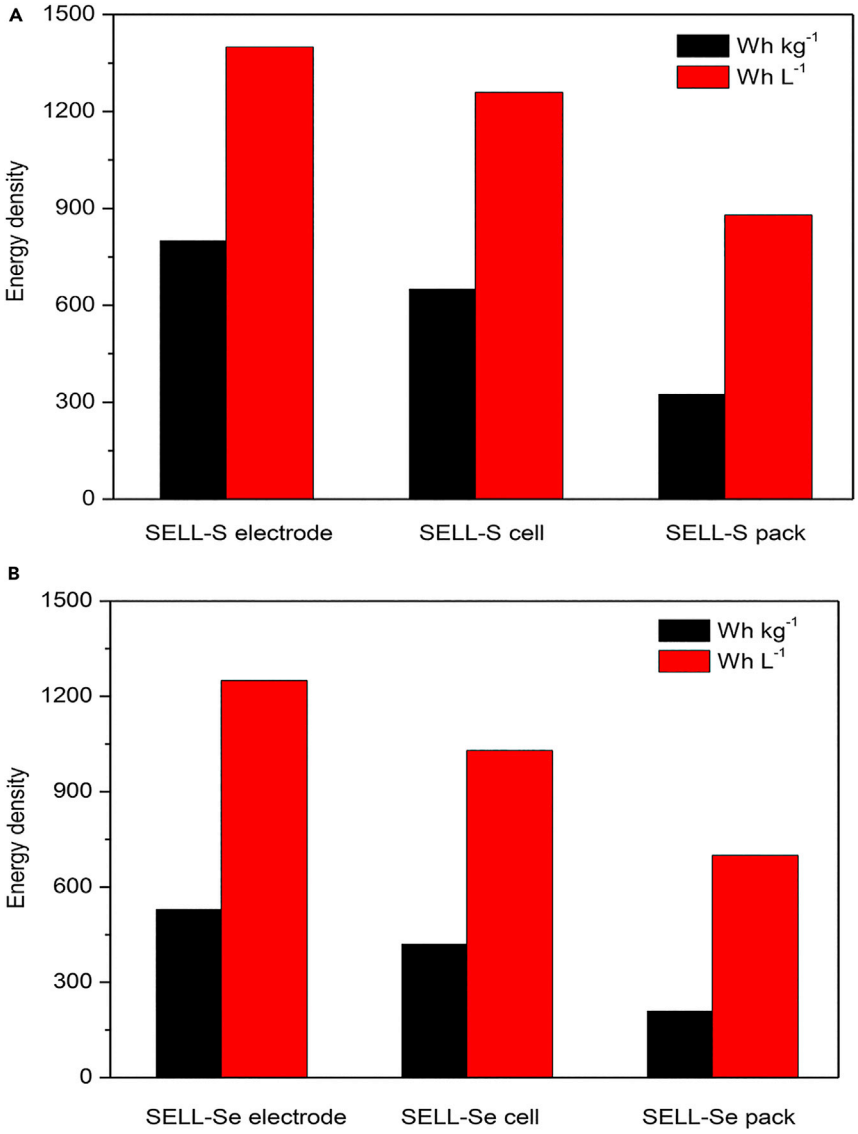

Figure 5. The Calculated Energy Density of SELL-S and SELL-Se Battery System

Energy density comparison of SELL-S (A) and SELL-Se (B) battery system at the electrode level, cell level, and pack level. Here, the densities of the stainless steel case were set as 8 g cm^{-3}.

Se cell, and the Coulombic efficiency can get more than 99% in the first cycle. The current density is about 10 mA cm^{-2}. It is noted that here we use limited Li source of 0.1 g, which means that 67% of the Li source is used (considering that the theoretical capacity of Li metal is 3,870 mAh g^{-1}).

DISCUSSION

By employing a solid garnet-type LLZTO tube electrolyte, we prepared a SELL-S and SELL-Se battery system with high energy density and superior electrochemical performance at 240°C–300°C. The assembled cells can achieve high Coulombic efficiency (99.99%, no shuttle effect), high power capability (up to 180 mW cm^{-2}), and high energy efficiency (>80%). In terms of cost, the energy cost of the current LLZTO tube is approximately \$30.1 kWh^{-1}, and by using LLZTO tube with larger diameter, its energy cost can be significantly reduced to less than \$10 kWh^{-1}

(Tables S2 and S3), which is much lower than that of the liquid organic electrolyte and separator (~$80 kWh^{-1}) in LIBs. The theoretical full electrode costs of the Li-S and Li-Se cells are estimated to be very low, $15 kWh^{-1} and $41 kWh^{-1}, respectively (Table S1), together with the low cost of the LLZTO tube, making it very possible for the total prices of the SELL-S and SELL-Se batteries to be lower than $100 kWh^{-1}. Overall, the low cost, high volume and mass energy density (Tables S4 and S5), and stable electrochemical performance of SELL-S and SELL-Se battery system makes them promising candidates for future concentrated and large-scale energy storage applications.

EXPERIMENTAL PROCEDURES

Fabrication and Characterization of the Garnet-type LLZTO Tubes

Li_2CO_3 (Sinopharm Chemical Reagent Co., Ltd, 99.99%), La_2O_3 (Sinopharm Chemical Reagent Co., Ltd, 99.99%), ZrO_2 (Aladdin, 99.99%), and Ta_2O_5 (Ourchem, 99.99%) powders were mixed together at a molar ratio of $Li_{6.5}La_3Zr_{0.5}Ta_{1.5}O_{12}$, ground with an agate mortar and pestle, and then heated at 900°C for 6 h to decompose the metal salts. The resulting powders were ball milled for 12 h before being pressed into a U-shaped tube with cold isostatic pressing at 330 MPa for 120 s and then annealed at 1,140°C for 16 h in air while the tube was covered with the same mother powder. All heat treatments were conducted in alumina crucibles (>99% Al_2O_3) covered with alumina lids.

The Archimedes water displacement method was used to measure the relative density of the LLZTO tube. XRD (Bruker AXS D8 Advance with Da Vinci) was used to monitor phase formation. The tube's microstructure was examined using a field-emission SEM (Shimadzu SSX-550). A broadband dielectric spectrometer (NOVOCOOL) was used to make the impedance spectroscopy measurements (frequency range, 40 Hz–10 MHz; AC voltage, 10 mV; and temperature range, 25°C–300°C).

The ionic conductivity of the LLZTO electrolyte is calculated based on a plain LLZTO pellet (Figure S5), which goes through the same isotactic pressing and calcination process as the LLZTO tube to make sure the same density and ionic conductivity. The thickness of the LLZTO pellet is about 1 mm. Then the LLZTO pellet surface was sputter coating with Au as an electrode for measurement.

Assembly and Electrochemical Measurements of the SELL-S and SELL-Se Cells

S (or Se) powders and carbon felt were first transferred to a stainless steel cell and heated for 3 h at 150°C (300°C) in a box furnace (MTI) to uniformly disperse the molten S (or Se) in the carbon felt (with a mass ratio of m(S or Se):m(C) = 9:1). Then, Li metal was placed into the garnet-type LLZTO tube and heated in a box furnace (MTI) at 240°C for 20 min to melt the Li metal. The LLZTO tube containing molten Li was then transferred into the stainless steel cell with the molten Se at 240°C. A 1-mm diameter stainless steel rod was inserted into the molten Li as the anode current collector. After the cell was cooled to room temperature, silicone rubber was used to seal the cell with a stainless steel cap. The whole assembly process was conducted in a glove box with an argon atmosphere.

The electrochemical performances of the SELL-S and SELL-Se cells were tested in an argon-filled box furnace (MTI) at 240°C and 300°C using a battery test system (LAND 2001 CT battery tester). The active surface area of each cell was 1 cm^2 as determined by the contact area between the LLZTO tube and the molten Li. The mass of active S in each cell is 10 mg and that of Se in each cell is 15 mg.

SUPPLEMENTAL INFORMATION

Supplemental Information can be found online at https://doi.org/10.1016/j.joule.2019.09.003.

ACKNOWLEDGMENTS

This work was supported by the National Natural Science Foundations of China (grants 51788104, 51661135025, 51807180, 51572145, and 51872159), National Basic Research of China (grant 2015CB932500), and China Postdoctoral Science Foundation.

AUTHOR CONTRIBUTIONS

Y.J., K.L., H.W., and Y.C. conceived the idea and co-wrote the manuscript. Y.J., K.L., J.L.L., X.J., Z.K.Z., Q.H.S., and Z.Y.H. carried out the materials synthesis and the electrochemical evaluation; Y.J., K.L., J.L.L., X.J., Z.K.Z., Q.H.S., Z.Y.H., Y.Z.L., C.-a.W., H.W., and Y.C. discussed the results and commented on the manuscript.

DECLARATION OF INTERESTS

The authors declare no competing interests.

Received: May 17, 2019
Revised: May 30, 2019
Accepted: September 4, 2019
Published: October 15, 2019

REFERENCES

1. Chu, S., Cui, Y., and Liu, N. (2016). The path toward sustainable energy. Nat. Mater. *16*, 16–22.
2. Sun, Y., Liu, N., and Cui, Y. (2016). Promises and challenges of nanomaterials for lithium-based rechargeable batteries. Nat. Energy *1*, 16071.
3. Dunn, B., Kamath, H., and Tarascon, J.M. (2011). Electrical energy for the grid: a battery of choices. Science *334*, 928–935.
4. Ji, X.L., Lee, K.T., and Nazar, L.F. (2009). A highly ordered nanostructured carbon-sulfur cathode for lithium-sulfur batteries. Nat. Mater. *8*, 500–506.
5. Abouimrane, A., Dambournet, D., Chapman, K.W., Chupas, P.J., Weng, W., and Amine, K. (2012). A new class of lithium and sodium rechargeable batteries based on selenium and selenium–sulfur as a positive electrode. J. Am. Chem. Soc. *134*, 4505–4508.
6. Manthiram, A., Fu, Y., and Su, Y.S. (2013). Challenges and prospects of lithium-sulfur batteries. Acc. Chem. Res. *46*, 1125–1134.
7. Xue, W., Shi, Z., Suo, L.M., Wang, C., Wang, Z.Q., Wang, H.Z., So, K.P., Maurano, A., Yu, D.W., Chen, Y.M., et al. (2019). Intercalation-conversion hybrid cathodes enabling Li–S full-cell architectures with jointly superior gravimetric and volumetric energy densities. Nat. Energy *4*, 374–382.
8. Jin, Y., Zhou, G., Shi, F., Zhuo, D., Zhao, J., Liu, K., Liu, Y., Zu, C., Chen, W., Zhang, R., et al. (2017). Reactivation of dead sulfide species in lithium polysulfide flow battery for grid scale energy storage. Nat. Commun. *8*, 462.
9. Yang, C.P., Yin, Y.X., and Guo, Y.G. (2015). Elemental selenium for electrochemical energy storage. J. Phys. Chem. Lett. *6*, 256–266.
10. Cui, Y., Abouimrane, A., Sun, C.J., Ren, Y., and Amine, K. (2014). Li-Se battery: absence of lithium polyselenides in carbonate based electrolyte. Chem. Commun. (Camb.) *50*, 5576–5579.
11. Cui, Y., Abouimrane, A., Lu, J., Bolin, T., Ren, Y., Weng, W., Sun, C., Maroni, V.A., Heald, S.M., and Amine, K. (2013). (De)Lithiation mechanism of Li/SeS_x (x=0~7) batteries determined by in situ synchrotron X ray diffraction and X ray absorption spectroscopy. J. Am. Chem. Soc. *135*, 8047–8056.
12. Yang, C.P., Xin, S., Yin, Y.X., Ye, H., Zhang, J., and Guo, Y.G. (2013). An advanced selenium carbon cathode for rechargeable lithium-selenium batteries. Angew. Chem. Int. Ed. *52*, 8363–8367.
13. Li, J., Zhang, C., Tao, Y., Ling, G., and Yang, Q. (2017). The Li-Se battery and its C/Se composite electrode: opportunities and challenges. Carbon *114*, 752.
14. Cai, Q., Li, Y., Wang, L., Li, Q., Xu, J., Gao, B., Zhang, X., Huo, K., and Chu, P.K. (2017). Freestanding hollow double-shell Se@CN x nanobelts as large-capacity and high-rate cathodes for Li-Se batteries. Nano Energy *32*, 1–9.
15. Zhang, J., Xu, Y., Fan, L., Zhu, Y., Liang, J., and Qian, Y. (2015). Graphene–encapsulated selenium/polyaniline core-shell nanowires with enhanced electrochemical performance for Li-Se batteries. Nano Energy *13*, 592–600.
16. Fang, R., Zhou, G., Pei, S., Li, F., and Cheng, H.M. (2015). Localized polyselenides in a graphene-coated polymer separator for high rate and ultralong life lithium-selenium batteries. Chem. Commun. (Camb.) *51*, 3667–3670.
17. Lee, J.T., Kim, H., Oschatz, M., Lee, D.C., Wu, F., Lin, H.T., Zdyrko, B., Cho, W.I., Kaskel, S., and Yushin, G. (2015). Micro-and mesoporous carbide-derive carbon-selenium cathodes for high-performance lithium selenium batteries. Adv. Energy Mater. *5*, 1400981.
18. Li, Z., Yuan, L., Yi, Z., Liu, Y., and Huang, Y. (2014). Confined selenium within porous carbon nanospheres as cathode for advanced Li-Se batteries. Nano Energy *9*, 229–236.
19. Jin, Y., Liu, K., Lang, J., Zhuo, D., Huang, Z., Wang, C., Wu, H., and Cui, Y. (2018). An intermediate temperature garnet-type solid electrolyte-based molten lithium battery for grid energy storage. Nat. Energy *3*, 732–738.
20. Thangadurai, V., Pinzaru, D., Narayanan, S., and Baral, A.K. (2015). Fast solid-state Li ion conducting garnet-type structure metal oxides for energy storage. J. Phys. Chem. Lett. *6*, 292–299.
21. Liu, K., and Wang, C. (2014). Garnet-type $Li_{6.4}La_3Zr_{1.4}Ta_{0.6}O_{12}$ thin sheet: fabrication and application in lithium–hydrogen peroxide semi-fuel cell. Electrochem. Commun. *48*, 147–150.

22. Liu, K., Ma, J., and Wang, C. (2014). Excess lithium salt functions more than compensating for lithium loss when synthesizing $Li_{6.5}La_3Ta_{0.5}Zr_{1.5}O_{12}$ in alumina crucible. J. Power Sources *260*, 109–114.

23. Thangadurai, V., Kaack, H., and Weppner, W.J.F. (2003). Novel fast lithium-ion conduction in garnet-type $Li_5La_3M_2O_{12}$ (M=Nb, Ta). J. Am. Ceram. Soc. *86*, 437–440.

24. Luo, W., Gong, Y., Zhu, Y., Li, Y., Yao, Y., Zhang, Y., Fu, K.K., Pastel, G., Lin, C.F., Mo, Y., et al. (2017). Reducing interfacial resistance between garnet-structured solid-state electrolyte and Li metal anode by a germanium layer. Adv. Mater. *29*, 1606042.

25. Fu, K., Gong, Y., Hitz, G.T., McOwen, D.W., Li, Y., Xu, S., Wen, Y., Zhang, L., Wang, C., Pastel, G., et al. (2017). Three-dimensional bilayer garnet solid electrolyte based high energy density lithium metal-sulfur batteries. Energy Environ. Sci. *10*, 1568–1575.

26. Ding, M.S., Xu, K., Zhang, S.S., Amine, K., Henriksen, G.L., and Jow, T.R. (2001). Change of conductivity with salt content, solvent composition, and temperature for electrolytes of $LiPF_6$ in ethylene carbonate-ethyl methyl carbonate. J. Electrochem. Soc. *148*, A1196–A1204.

27. Meridian International Research. (2005). Battery Technologies. In Seven Six, The sodium/nickel chloride "Zebra" battery-Battery technology, pp. 104–112.

28. Sudworth, J.L. (2001). The sodium/nickel chloride (ZEBRA) battery. J. Power Sources *100*, 149–163.

29. Hueso, K.B., Armand, M., and Rojo, T. (2013). High temperature sodium batteries: status, challenges and future trends. Energy Environ. Sci. *6*, 734–749.

30. Skyllas-Kazacos, M., Chakrabarti, M.H., Hajimolana, S.A., Mjalli, F.S., and Saleem, M. (2011). Progress in flow battery research and development. J. Electrochem. Soc. *158*, R55–R79.

31. Peng, J., Zu, C., and Li, H. (2013). Fundamental scientific aspects of lithium batteries (I) thermodynamic calculations of theoretical energy densities of chemical energy storage systems. Energ Stor Sci Technol *2*, 55–62.

32. Wen, Z., Cao, J., Gu, Z., Xu, X., Zhang, F., and Lin, Z. (2008). Research on sodium sulfur battery for energy storage. Solid State Ion. *179*, 1697–1701.